Electronic Supplementary Information

Influence of the Hydrophobic Domain on the Self-Assembly and Hydrogen Bonding of Hydroxy-Amphiphiles

Valery Andrushchenko* and Walter Pohle*

Content

Computational procedures

References

Computational procedures

Octadecanol computations

<u>Starting geometries.</u> An initial geometry of ODA (Figure 1) was obtained from the Human Metabolome Database.[1] The initial geometries for methanol (MA), ethanol (EA), butanol (BA), decanol (DA), and their assemblies, as well as the starting structures for the MD simulations were generated with the aid of MCM software.[2] The initial geometries for the structures of the assemblies were created according to the XRD data of Abrahamsson *et al.*[3] to meet the prerequisites for hydrogen-bond (H-bond) formation between the monolayers. For the quantum-mechanical (QM) and semi-empirical calculations of the model bilayers, one of the monolayers was constituted of trans conformers of the alcohol, while the other one was constituted of *gauche* conformers. The geometries of the longer systems $(MA)_{40}$, $(EA)_{40}$ and $(MA)_{200}$ were obtained by propagating $(MA)_{10}$ or $(EA)_{10}$ four or 20 times, respectively. Furthermore, $(EA)_{10}$ and ODA assemblies were also investigated with trans conformers in both monolayers. For the MD simulations of ODA each monolayer had 49 molecules (forming a $7{\times}7$ lattice) resulting in a total of 98 molecules in the bilayer assembly. Systems with both γ- and β-form structures were generated and subjected to MD simulations.

<u>MD simulations.</u> All MD simulations were done with Amber 9 package[4] using supplied general amber force field (GAFF). Although this force field was not specifically developed for lipid or hydrocarbon applications, several tests suggest its good applicability to such systems, comparable to CHARMM27 and GROMOS.[5-7] Atomic charges were assigned for both trans (**t**) and *gauche* (**g**) ODA conformers using the RESP potential fit method[8] with the aid of *antechamber* module from Amber 9 package and GAUSSIAN 09 software package[9] (Tables S3 and S4).

Periodic boundary conditions (PBC) were used for all the simulations. The size of the single PBC cell was set by *tleap* module of Amber 9 using Van-der-Waals box dimensions. The starting structure consisting of 98 ODA molecules was first subjected to 2500 steps of initial minimization to relax possible bad geometrical contacts (1000 steps with steepest descent and the rest with conjugate gradient algorithms) with a 12 Å cut-off of Lennard-Jones interactions. The initial minimization was followed by the heating of the system from 0 to 295 K in the NVT ensemble for 20 ps and by subsequent equilibration at 295 K in the NPT ensemble for 100 ps. Finally, the 20 ns production run was performed at 295 K in the NPT ensemble. Both equilibration and production steps were done with 10 Å cut-off using Langevin dynamics with the collision frequency γ=1 and employing SHAKE algorithm on the hydrogen atoms with a tolerance of 10^{-5} Å and 2 fs time step. The particle mesh Ewald method (PME) was used for handling long-range electrostatic interactions. The resulting PBC box sizes were $48.6 \times 32.7 \times 29.8$; $48.8 \times 31.7 \times 30.5$ and $47.5 \times 32.4 \times 29.1$ Å^3 for trans-*gauche* (**tg**) and trans-trans (**tt**) models of γ-form, and for β-form, respectively.

For the simulation of bilayer hydration, the system $(ODA)_{98}$ was surrounded by a shell containing either one (representing 10 % hydration level) or 10 (representing full hydration) water molecules per

amphiphile, using *tleap* module of Amber 9 (Figure S11). The TIP3P force field[10] was used for water. Initially, three stages of restrained minimization were done to relax possible bad geometrical contacts between water and ODA molecules. Each stage consisted of 500 steps of minimization with steepest descent algorithm followed by 500 steps of minimization with conjugate gradient algorithm and the ODA atoms fixed with force constants of 80, 40, and 2 kcal/(mol Å^2) at each stage, respectively. Then unrestrained minimization was performed with 1000 steps of steepest descent and 1500 steps of conjugate gradient algorithms. Hereafter, the system was heated from 0 to 295 K in the NVT ensemble within 20 ps, keeping the ODA atoms fixed with a force constant of 10 kcal/(mol Å^2). The heating was followed by 100 ps of NPT equilibration at 295 K without any restraints. Finally, the 20 ns production run was performed at 295 K in the NPT ensemble. All other parameters of the simulation were the same as described above for the non-hydrated systems. For the systems with one water molecule per amphiphile, the resulting PBC box sizes were $46.7 \times 35.4 \times 29.3$, $48.0 \times 32.7 \times 30.9$ and $53.2 \times 32.0 \times 28.1$ Å^3 for trans-*gauche* (**tg**) and trans-trans (**tt**) models of γ-form, and for β-form, respectively. The box size for **tg** model with 10 water molecules per amphiphile was $45.2 \times 51.3 \times 32.9$ Å^3.

QM calculations. All QM calculations were performed with GAUSSIAN 09 software package.[9] The initial structures for MA, $(MA)_2$, $(MA)_3$, $(MA)_{10}$, EA, $(EA)_2$, $(EA)_3$ and $(EA)_{10}$ were optimized in vacuum by an energy minimization with B3LYP functional[11] and the Pople-type 6-31++G** basis set. We consider the vacuum approximation appropriate as the experimental IR data are obtained in dry films. For the optimized structures, harmonic vibrational frequencies and IR intensities were calculated. The anharmonic effects were neglected. Although anharmonic corrections can significantly shift νCH and νOH bands,[12] we supposed that the anharmonic effects are still smaller than the harmonic coupling as long as the bands are well separated. Indeed, as it will be shown below, the harmonic approximation provided the most important spectral features observed experimentally. Frequency scaling was not performed.

For the $(MA)_{10}$ and $(EA)_{10}$, a plane symmetry (C_s) was used as previously applied to ethanol systems.[13] All the other structures were fully optimized without any symmetry restrictions. The larger BA and DA systems were optimized at a semi-empirical PM3 level including the computations of IR frequencies and intensities. In order to obtain the IR spectra of larger hydrogen-bonded systems, which are not applicable to direct QM calculations, the force field and intensity tensors [14-16] of $(MA)_{40}$, $(EA)_{40}$ and $(MA)_{200}$ were constructed from the $(MA)_{10}$ or $(EA)_{10}$ fragments, respectively, by applying the Cartesian coordinate transfer (CCT) technique[17, 18]. To generate the spectra with finite bandwidth, the computed line spectra were extracted from the GAUSSIAN 09 output and convoluted with Lorentzian curves with bandwidth of 10 cm^{-1} using a set of home-built programs.

Dioleoylglycerol computations

A multi-scale MD/DFT approach[19, 20] accounting for the conformational and dynamic effects was applied to the DOG system.

<u>MD simulations.</u> An initial geometry for the DOG molecule (Figure 1) was created using MCM program[2]. Ten DOG molecules ($(DOG)_{10}$) were put randomly inside a cube with 35 Å side dimension (avoiding intermolecular clashing) by means of Packmol program[21] and subjected to 10 ns of Generalized Born (GB) MD run. The GB approach is appropriate for water-depleted DOG with implicit solvent simulating the bulk DOG molecules around the ten explicit ones. Both GB and PBC simulations with different initial arrangement of individual molecules (random, bilayer, micellar) were shown to converge to very similar assembly structures.[22] The ensemble size of $(DOG)_{10}$ is considered as realistic resulting from our preceding simulations with $(DOG)_6$ and $(DOG)_{60}$ systems.[22] All MD simulations were done with Amber 9 package[4] using GAFF forcefield. Atomic charges for the DOG molecule were assigned semi-empirically with the help of *antechamber* module from Amber 9 package, which, in this case, makes use of *divcon* program and AM1-BCC (Bond Charge Correction) method for charge calculation (Table S5).[4] Because DOG is very flexible and can exist in multiple configurations, it is more suitable to use the BCC method, computing the average charge without accounting for a particular conformation. The RESP charge fitting would require in this case QM calculations for a very large number of possible DOG configurations. All simulations were done with dielectric constant $\varepsilon=2.0$ (value for carbohydrates approximately representing the bulk DOG molecules), with GB model II[23] employing the Analytical Linearized Poisson-Boltzmann (ALPB) model.[24] This model provides higher accuracy for the treatment of the electrostatic interactions in the case of finite solvent dielectric constants compared to standard GB. Effective electrostatic size (radius) of the molecule was estimated by the *elsize* utility from the Amber 9 package to be 6.94 Å. The constructed ensemble of 10 DOG molecules was first subjected to 2500 steps of initial minimization to relax possible bad geometrical contacts (1000 steps with steepest descent and the rest with conjugate gradient algorithms) with no cut-off. The initial minimization was followed by 20 ps of equilibration with the system heated from 0 to 300 K. The 10 ns production run was performed at 300 K. Both equilibration and production steps were done with a 50 Å cut-off of Lennard-Jones interactions, using Langevin dynamics with the collision frequency $\gamma=1$ and employing SHAKE algorithm on H atoms with a tolerance of 10^{-5} Å and 2 fs time step. The results of the MD simulations, including the analysis of H-bonds, were treated with the *ptraj* utility from the Amber 9 package. Further analysis of the *ptraj* output was done by a home-built program "Ptraj HBOND"[25].

The resulting geometries of six random MD snapshots and the lowest potential energy structure were used for further QM calculations. All DOG molecules in the ensemble were classified in two types, which comprise either hydrogen-bonded (inter- or intramolecularly) or free species. A total of 14 free and 8 H-bonded molecules with different H-bond patterns were used for QM calculations. The H-bonded molecules were further classified according to the bonding pattern.

QM calculations. For all the molecules, the hydrocarbon tails, less essential in this case, were truncated so that only the capping methyl groups were left. Such a reduction of the molecular size allowed us to perform high-level DFT computations necessary for the correct representation of vibrational frequencies. The molecular fragments were subjected to full DFT optimization and frequency calculations with GAUSSIAN 09 in vacuum at the B3LYP/6-31++G** level. Two H-bonded molecules were considered and computed as one system. Altogether, 22 DFT calculations were done. Since the resulting MD structures were close to the local minima, the geometry of the fragments did not change significantly during the QM optimization procedure.

Infrared spectra were generated for all the fragments from the GAUSSIAN 09 frequency calculation output using Lorentzian bands with a width of 10 cm^{-1} utilizing a set of home-built programs. Frequency scaling was not performed. The spectra were averaged in three steps as illustrated in Figure S12. First, the spectra of the systems with the same H-bond pattern as well as the spectra of free molecules were time-averaged with equal weight to represent the dynamics of the system. In the second step, the time-averaged spectra for the H-bonded species were weighted according to their relevant occurrence obtained in the course of the MD run (see Table 4, 3rd column). And finally, the weighted spectrum of the H-bonded molecules and the averaged spectrum of the free species were again weighted according to their occurrence obtained in the MD run (see Table 4, 2nd column). The final result was then compared with the experimental DOG spectrum.

Detailed analysis of the calculated IR spectra of ethanol models

The two H-bonded ethanol molecules of (EA)$_2$ (note that the H donor molecule is in trans conformation while the acceptor is in *gauche* conformation) have two separate bands at 3819 and 3669 cm^{-1} arising from free (coming from the *gauche* conformer) and H-bonded (from the trans conformer) OH groups, respectively (Figures 4 and S7). The free OH group vibrates at higher frequency compared to the H-bonded one and has a much lower intensity as it was shown before.[26] The presence of the two H-bonds in (EA)$_3$ leads to coupling of the νOH vibrations of the H-bonded groups. This results in appearance of two coupled modes at 3592 and 3550 cm^{-1}, corresponding to out-of-phase and in-phase coupled vibrations, respectively. The dipole moments of these modes are nearly perpendicular to each other (Figure S7). The highest-frequency mode at 3832 cm^{-1} arises from the free OH group of one of the trans conformers.

The coupling of the νOH modes of different molecules in (EA)$_{10}$ gives rise to several out-of-phase and in-phase vibrations (Figure 4 and Table 2). As for methanol, the splitting into multiple bands can be referred to end effects. Vibrational displacements for the most intense bands at 3585 and 3508 cm^{-1} are illustrated in Figure S7.

The IR spectrum of (EA)$_{10}$ with **tg** conformation of the monomers is largely similar to its counterpart with **tt** conformers (Figure 4). The multiple-split bands converge in the spectrum of (EA)$_{40}$ into two main νOH peaks at 3586 and 3498 cm^{-1}, corresponding to out-of-phase and in-phase coupled vibrations, respectively (Figures 4 and S7). There is a considerable difference between these latter two

wavenumbers compared to the corresponding values for $(MA)_{40}$ by about 85 cm^{-1} on average. As in the methanol models, the integral intensity of the H-bonded νOH bands and the magnitude of the static dipole moment linearly increase with the number of H-bonded monomeric units in the system (Figures S5 and S6), suggesting the absence of cooperative effects in the formation of the H-bond network.

The dipole moments of the coupled out-of-phase and in-phase modes are nearly perpendicular to each other for all the studied ethanol systems (Figure S7), as for methanol. The computed geometrical parameters (bond lengths and angles) for $(EA)_{10}$ (Table 2) generally agree well with crystal-XRD data.[3] One exception is the O-C-C angle in the *gauche* conformers (113.32°), which is larger than that obtained by XRD (109.18°), whereas that angle is in perfect agreement with experimental data for the trans conformer (109.2°). However, the *gauche* conformer has an intrinsically larger value of the O-C-C angle close to 113°, as can be seen for *gauche* EA monomer and the *gauche* conformers in $(EA)_2$ and $(EA)_3$ (Table 2) and also from literature data[13].

Table S1. Peak wavenumbers for νOH bands arising from several compounds; values for the films measured in our laboratory were obtained at relative humidity of 0 %.

Compound [a]	Physical State	Wavenumber(s), cm⁻¹		Reference
Octadecanol	Solution in CCl_4	3638		AIST
	Film	3288 sh	3227	this paper
	Film	3285	3210	Batishcheva[27]
	Nujol	3311	3230 [b]	Aldrich
	Resolidified [c]	3330	3250 sh	Tasumi[28]
	KBr	3380 [b] sh	3304	AIST
Eicosanol	Nujol	3320 [b] sh	3229	Aldrich
Hexadecanol	Nujol	3310 [b]	3260 [b]	AIST
2-Hexadecanol	Nujol	3350 [b]	3300 [b]	AIST
Tetradecanol	Nujol	3300 [b] sh	3230	AIST
Tetradecanol	Film	3300	3210	Batishcheva[27]
Dioleoylglycerol	Fluid film	3515	3465	this paper
Oleyl alcohol	Neat; liquid film	3322; 3332		Aldrich; AIST
Heptadecanol	Resolidified [c]	3300		Tasumi[28]
Hexadecanol	Melt	3340		Aldrich
2-Hexadecanol	Melt	3359		Aldrich
Dodecanol	Nujol	3328		AIST
Octanol, Hexanol	Neat	3329		Aldrich
2-Octanol	Neat	3345		Aldrich
Butanol, Ethanol	Neat	3333 ± 2		Aldrich
2-Butanol	Neat	3343; 3353		Aldrich; AIST
2-Methyl-2-propanol	Neat	3362; 3366		Aldrich; AIST
Heptanol, Pentanol, Propanol	Neat	3324 ± 1		Aldrich
2-Propanol	Neat	3342; 3340		Aldrich; AIST
Methanol	Neat	3336; 3347		Eysel[29]; AIST
Methanol	Neat	3342		Aldrich
22-Hydroxybehe-nylphosphocholine	Film	3290		Pohle[30]
Water	Liquid	3390 ± 10		own data

[a] Compounds are the primary (n-)alcohols in each case, if not specified otherwise.

[b] These wavenumbers were estimated (rounded to the next decade) from the catalogue spectra (Aldrich[31] and AIST[32]) since the explicit values were not provided there.

[c] Rapidly resolidified after melting.

Table S2. Main geometrical parameters for optimized (B3LYP/6-31++G**) methanol models and vibrational assignments in the νOH region; the individual molecules in (MA)$_2$ and (MA)$_3$, structures are labeled with subscript indices as shown in Figure 3 in the main text.

Fragment	Wavenumber, cm^{-1}	Assignment	C-O bond length, Å	O-H bond length, Å	O···O distance, Å	H-bond length, Å	O-H···O angle, °
MA	3839	localized νOH	1.426	0.965	-	-	-
(MA)$_2$	3838w	localized νOH of MA$_1$ (free)	1.433 (MA$_1$)	0.966 (MA$_1$)			
	3675	localized νOH of MA$_2$ (H-bonded)	1.419 (MA$_2$)	0.974 (MA$_2$)	2.867	1.896	175
(MA)$_3$	3847w	localized νOH of MA$_1$ (free)	1.44 (MA$_1$)	0.965 (MA$_1$)			
	3604	coupled νOH of MA$_2$ and MA$_3$, out of phase	1.425 (MA$_2$)	0.979 (MA$_2$)	2.789 (MA$_1$···MA$_2$)	1.826 (MA$_1$···MA$_2$)	167 (MA$_1$···MA$_2$)
	3555	coupled νOH of MA$_2$ and MA$_3$, in phase	1.418 (MA$_3$)	0.979 (MA$_3$)	2.797 (MA$_2$···MA$_3$)	1.836 (MA$_2$···MA$_3$)	166 (MA$_2$···MA$_3$)
(MA)$_{10}$	3847w	localized νOH of the only free OH group					
	3633m, 3612m, 3535	coupled νOH, out of phase					
	3512m	coupled νOH, out of phase mixed with in phase					
	3477m, 3417	coupled νOH, in phase	1.422 (av) ^{a}	0.980 (av)	2.756 (av)	1.774 (av)	180 (av)
(MA)$_{40}$ ^{b}	3847w	localized νOH of the only free OH group					
	3521m	coupled νOH, out of phase					
	3401	coupled νOH, in phase	-	-	-	-	-

^{a} "(av)" stands for average.
^{b} This structure could not be optimized due to large system size.

Table S3. Atomic charges for a trans ODA conformer determined with the RESP potential fit method[8].

Atom number	Atom name	Coordinates			Charge
		X	Y	Z	
1	C	8.424	-13.598	0	0.3156
2	C1	7.162	-12.718	0	0.0868
3	C2	5.912	-13.617	0	-0.1174
4	C3	4.65	-12.737	0	0.074
5	C4	3.4	-13.634	0	0.0935
6	C5	2.137	-12.756	0	-0.0037
7	C6	0.889	-13.654	0	0.0358
8	C7	-0.373	-12.777	0	0.0608
9	C8	-1.622	-13.676	0	0.0234
10	C9	-2.885	-12.799	0	0.038
11	C10	-4.133	-13.699	0	0.0575
12	C11	-5.397	-12.823	0	0.015
13	C12	-6.644	-13.725	0	0.0349
14	C13	-7.909	-12.85	0	0.0933
15	C14	-9.154	-13.753	0	-0.0185
16	C15	-10.421	-12.879	0	0.0032
17	C16	-11.666	-13.782	0	0.1936
18	C17	-12.934	-12.907	0	-0.2823
19	O	9.586	-12.765	0	-0.741
20	H	8.429	-14.175	0.817	-0.0348
21	H1	8.429	-14.176	-0.816	-0.0348
22	H2	7.157	-12.142	0.816	0.0111
23	H3	7.156	-12.141	-0.817	0.0111
24	H4	5.916	-14.194	-0.817	0.0108
25	H5	5.916	-14.194	0.817	0.0108
26	H6	4.645	-12.159	0.816	-0.0265
27	H7	4.645	-12.16	-0.817	-0.0265
28	H8	3.405	-14.212	-0.817	-0.0279
29	H9	3.405	-14.212	0.817	-0.0279
30	H10	2.134	-12.178	0.818	-0.0109
31	H11	2.134	-12.179	-0.817	-0.0109
32	H12	0.894	-14.232	-0.816	-0.0196
33	H13	0.894	-14.232	0.816	-0.0196
34	H14	-0.379	-12.199	0.818	-0.0227
35	H15	-0.379	-12.199	-0.816	-0.0227
36	H16	-1.617	-14.253	-0.817	-0.0167
37	H17	-1.617	-14.254	0.816	-0.0167

38	H18	-2.891	-12.222	0.818	-0.0192
39	H19	-2.891	-12.221	-0.816	-0.0192
40	H20	-4.127	-14.276	-0.816	-0.0229
41	H21	-4.127	-14.276	0.816	-0.0229
42	H22	-5.402	-12.245	0.817	-0.0155
43	H23	-5.403	-12.246	-0.817	-0.0155
44	H24	-6.638	-14.302	-0.816	-0.0177
45	H25	-6.638	-14.302	0.817	-0.0177
46	H26	-7.916	-12.273	0.817	-0.0295
47	H27	-7.915	-12.273	-0.816	-0.0295
48	H28	-9.147	-14.33	-0.816	-0.0116
49	H29	-9.147	-14.33	0.817	-0.0116
50	H30	-10.426	-12.302	0.817	-0.0071
51	H31	-10.426	-12.301	-0.817	-0.0071
52	H32	-11.66	-14.359	-0.817	-0.0347
53	H33	-11.659	-14.359	0.816	-0.0347
54	H34	-13.744	-13.494	0	0.0615
55	H35	-12.94	-12.33	-0.817	0.0615
56	H36	-12.94	-12.33	0.816	0.0615
57	H37	10.407	-13.336	0	0.4438

Table S4. Atomic charges for a *gauche* ODA conformer determined with the RESP potential fit method[8].

Atom number	Atom name	Coordinates			Charge
		X	Y	Z	
1	C	13.047	-13.893	0	0.368
2	C1	14.325	-14.722	0	-0.1269
3	C2	15.593	-13.867	0	-0.0322
4	C3	16.877	-14.697	0	0.1443
5	C4	18.147	-13.844	0	0.0192
6	C5	19.432	-14.673	0	0.0035
7	C6	20.702	-13.82	0	0.0645
8	C7	21.988	-14.648	0	0.0408
9	C8	23.258	-13.795	0	0.0204
10	C9	24.544	-14.624	0	0.0485
11	C10	25.814	-13.771	0	0.0529
12	C11	27.1	-14.6	0	0.0129
13	C12	28.37	-13.747	0	0.0369
14	C13	29.656	-14.575	0	0.0942
15	C14	30.926	-13.722	0	-0.0201
16	C15	32.212	-14.551	0	0.0043
17	C16	33.483	-13.699	0	0.1931
18	C17	34.763	-14.534	0	-0.2828
19	O	11.881	-14.68	0	-0.7091
20	H	13.024	-13.25	0.875	-0.0089
21	H1	13.024	-13.25	-0.875	-0.0089
22	H2	14.322	-15.371	0.875	0.0302
23	H3	14.322	-15.371	-0.875	0.0302
24	H4	15.586	-13.214	-0.871	-0.0029
25	H5	15.586	-13.214	0.871	-0.0029
26	H6	16.883	-15.35	0.871	-0.0371
27	H7	16.883	-15.35	-0.871	-0.0371
28	H8	18.14	-13.19	-0.871	-0.0138
29	H9	18.14	-13.19	0.871	-0.0138
30	H10	19.439	-15.326	0.871	-0.0134
31	H11	19.439	-15.326	-0.871	-0.0134
32	H12	20.696	-13.166	-0.871	-0.0229
33	H13	20.696	-13.166	0.871	-0.0229
34	H14	21.994	-15.302	0.871	-0.019
35	H15	21.994	-15.302	-0.871	-0.019
36	H16	23.252	-13.142	-0.871	-0.0163
37	H17	23.252	-13.142	0.871	-0.0163

| 38	H18	24.55	-15.278	0.871	-0.0209
39	H19	24.55	-15.278	-0.871	-0.0209
40	H20	25.808	-13.117	-0.871	-0.0218
41	H21	25.808	-13.117	0.871	-0.0218
42	H22	27.106	-15.253	0.871	-0.0153
43	H23	27.106	-15.253	-0.871	-0.0153
44	H24	28.364	-13.093	-0.871	-0.0179
45	H25	28.364	-13.093	0.871	-0.0179
46	H26	29.662	-15.229	0.871	-0.0296
47	H27	29.662	-15.229	-0.871	-0.0296
48	H28	30.92	-13.069	-0.871	-0.0114
49	H29	30.92	-13.069	0.871	-0.0114
50	H30	32.219	-15.205	0.871	-0.0073
51	H31	32.219	-15.205	-0.871	-0.0073
52	H32	33.478	-13.046	-0.87	-0.0344
53	H33	33.478	-13.046	0.87	-0.0344
54	H34	35.646	-13.902	0	0.0617
55	H35	34.814	-15.173	-0.877	0.0617
56	H36	34.814	-15.173	0.877	0.0617
57	H37	12.106	-15.598	0.002	0.4082

Table S5. Atomic charges for a DOG molecule determined with *divcon* program using AM1-BCC semi-empirical method[4].

Atom number	Atom name	Coordinates			Charge
		X	Y	Z	
1	O1	15.816	21.758	21.992	-0.4365
2	O2	14.051	19.45	22.845	-0.4386
3	O3	15.863	23.933	21.31	-0.5625
4	O4	13.638	17.465	21.811	-0.5415
5	O5	13.441	23.731	22.422	-0.607
6	C6	17.942	22.22	25.092	-0.0856
7	C7	17.287	22.023	26.495	-0.0802
8	C8	12.329	19.295	26.102	-0.0808
9	C9	11.384	20.494	26.247	-0.0794
10	C10	18.247	23.021	32.173	-0.0804
11	C11	16.799	22.697	32.669	-0.0793
12	C12	15.037	25.819	27.918	-0.0846
13	C13	15.12	25.71	26.326	-0.0794
14	C14	17.77	23.653	24.601	-0.0857
15	C15	17.418	20.482	26.842	-0.0723
16	C16	11.79	18.268	25.11	-0.0833
17	C17	19.285	23.607	33.174	-0.0795
18	C18	11.939	21.558	27.204	-0.0745
19	C19	16.193	26.697	28.482	-0.0786
20	C20	16.037	21.737	31.751	-0.0731
21	C21	14.034	24.858	25.665	-0.0779
22	C22	18.373	23.902	23.138	-0.074
23	C23	17.041	20.243	28.399	-0.0507
24	C24	12.721	17.105	24.959	-0.0749
25	C25	20.522	24.065	32.538	-0.08
26	C26	16.604	26.376	29.925	-0.0812
27	C27	11.128	22.838	27.258	-0.0449
28	C28	15.763	22.333	30.365	-0.0517
29	C29	12.658	25.382	25.911	-0.0481
30	C30	17.883	22.937	21.991	-0.1272
31	C31	21.437	24.819	33.46	-0.0801
32	C32	17.66	27.386	30.51	-0.0789
33	C33	14.024	17.411	24.159	-0.1269
34	C34	15.52	20.405	28.679	-0.1709
35	C35	15.02	21.249	29.564	-0.1698
36	C36	10.961	23.427	25.906	-0.1782

37	C37	11.583	24.457	25.322	-0.1614
38	C38	16.438	22.912	21.727	0.6438
39	C39	14.348	21.635	21.78	0.107
40	C40	22.685	25.432	32.791	-0.0926
41	C41	19.009	27.369	29.775	-0.0938
42	C42	13.89	18.105	22.823	0.6364
43	C43	13.963	20.148	21.598	0.1411
44	C44	13.533	22.375	22.882	0.1173
45	H45	19.015	22.042	25.188	0.0377
46	H46	17.485	21.471	24.442	0.051
47	H47	17.812	22.664	27.208	0.0397
48	H48	16.255	22.375	26.463	0.0496
49	H49	13.339	19.608	25.826	0.0411
50	H50	12.382	18.85	27.098	0.0388
51	H51	11.214	20.973	25.281	0.048
52	H52	10.395	20.145	26.55	0.0389
53	H53	18.732	22.074	31.925	0.0393
54	H54	18.143	23.791	31.405	0.0402
55	H55	16.936	22.162	33.611	0.0398
56	H56	16.178	23.572	32.869	0.0406
57	H57	14.043	26.159	28.215	0.0406
58	H58	15.107	24.851	28.419	0.0451
59	H59	15.099	26.729	25.934	0.0406
60	H60	16.084	25.254	26.09	0.036
61	H61	16.725	23.824	24.338	0.0463
62	H62	18.085	24.422	25.31	0.048
63	H63	16.656	19.919	26.298	0.0381
64	H64	18.407	20.061	26.654	0.0382
65	H65	10.862	17.806	25.453	0.0464
66	H66	11.547	18.826	24.204	0.047
67	H67	18.787	24.506	33.544	0.0401
68	H68	19.415	22.854	33.953	0.0396
69	H69	11.9	21.109	28.198	0.0351
70	H70	12.981	21.777	26.959	0.045
71	H71	17.086	26.572	27.866	0.0379
72	H72	15.883	27.728	28.293	0.0394
73	H73	16.69	20.887	31.543	0.0424
74	H74	15.163	21.259	32.197	0.0414
75	H75	14.279	24.781	24.603	0.0478
76	H76	14.071	23.823	26.012	0.0396
77	H77	18.077	24.887	22.771	0.0581

|					
78	H78	19.465	23.885	23.161	0.0518
79	H79	17.274	19.194	28.597	0.0464
80	H80	17.618	20.973	28.969	0.0489
81	H81	13.071	16.8	25.947	0.0522
82	H82	12.159	16.31	24.465	0.0575
83	H83	21.109	23.18	32.283	0.0391
84	H84	20.323	24.622	31.622	0.0395
85	H85	15.738	26.475	30.583	0.0376
86	H86	17.013	25.366	30.003	0.0412
87	H87	10.162	22.73	27.754	0.0413
88	H88	11.654	23.551	27.898	0.0433
89	H89	15.032	23.13	30.518	0.0459
90	H90	16.701	22.681	29.927	0.0473
91	H91	12.422	25.425	26.976	0.042
92	H92	12.529	26.398	25.535	0.0472
93	H93	18.312	23.196	21.021	0.0793
94	H94	18.157	21.884	22.095	0.0808
95	H95	20.858	25.61	33.943	0.0388
96	H96	21.733	24.104	34.23	0.0386
97	H97	17.286	28.404	30.389	0.0397
98	H98	17.838	27.276	31.583	0.0369
99	H99	14.614	18.053	24.817	0.0785
100	H100	14.605	16.5	23.994	0.0774
101	H101	14.86	19.886	27.987	0.1175
102	H102	13.941	21.354	29.492	0.119
103	H103	10.223	22.912	25.295	0.1165
104	H104	11.143	24.701	24.358	0.1321
105	H105	14.069	21.993	20.786	0.0845
106	H106	22.388	26.141	32.015	0.0323
107	H107	23.315	24.669	32.328	0.0323
108	H108	23.3	25.932	33.542	0.0328
109	H109	19.534	26.425	29.938	0.0327
110	H110	19.779	28.097	30.04	0.0319
111	H111	18.823	27.426	28.7	0.0324
112	H112	14.608	19.684	20.847	0.0737
113	H113	12.942	20.082	21.215	0.0639
114	H114	14.024	22.309	23.856	0.0444
115	H115	12.574	21.851	22.909	0.0833
116	H116	14.287	24.167	22.217	0.4223
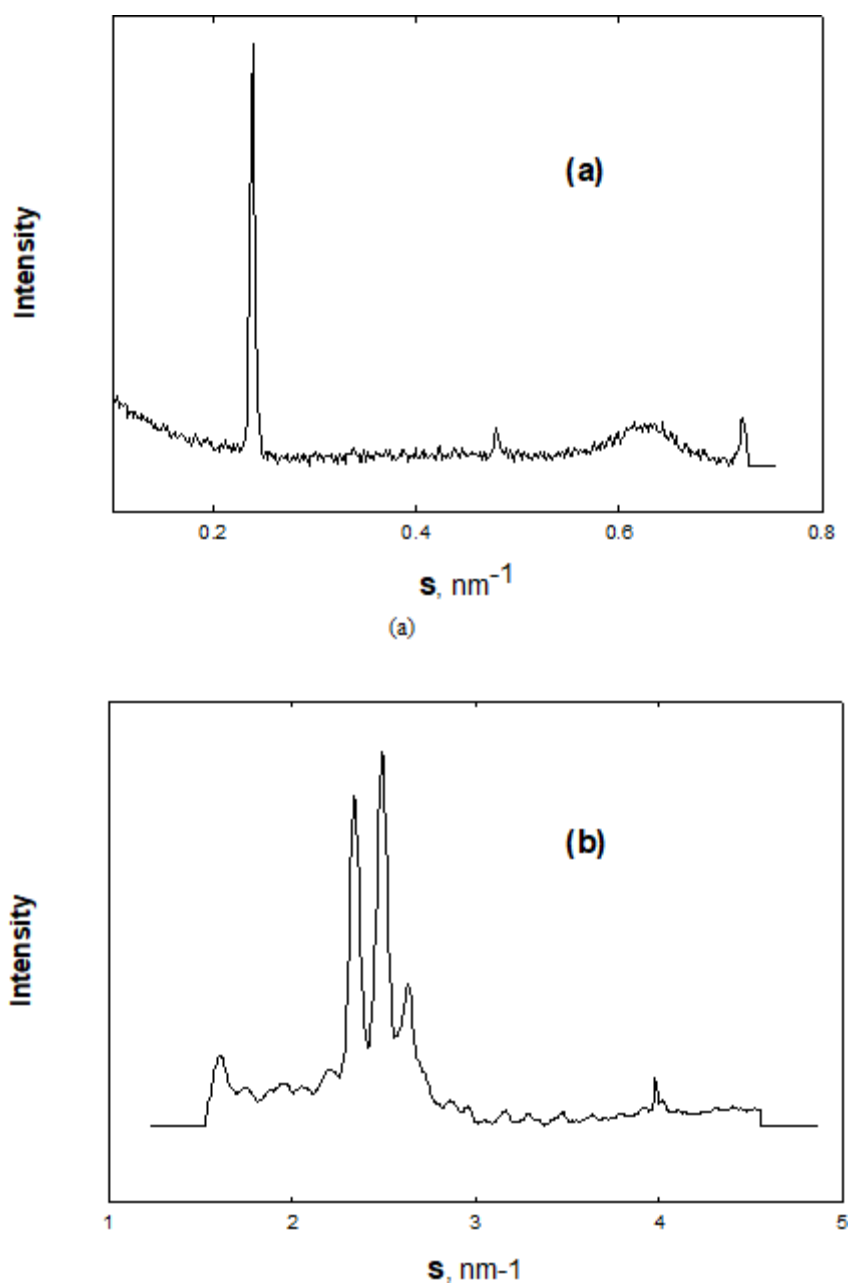
Figure S1. XRD patterns obtained for films of ODA at 0 % RH in the small-angle (SAXS, **a**) and wide-angle (WAXS, **b**) scattering regions.
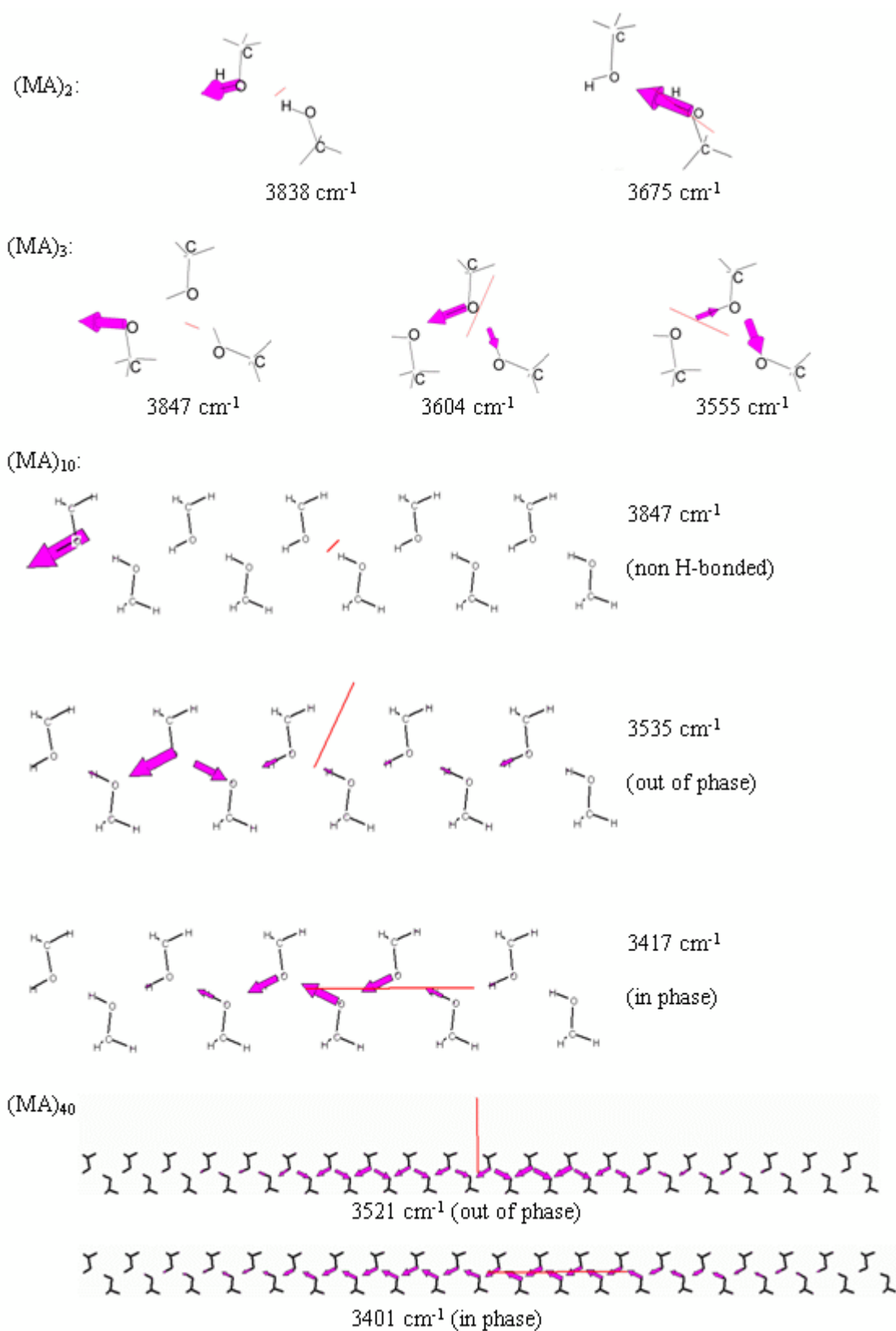
Figure S2. Displacements of selected vibrations due to the νOH normal mode (thick magenta arrows) in systems composed of two, three, ten and 40 methanol molecules; the red lines show the directions of resulting O-H transition dipole moments.
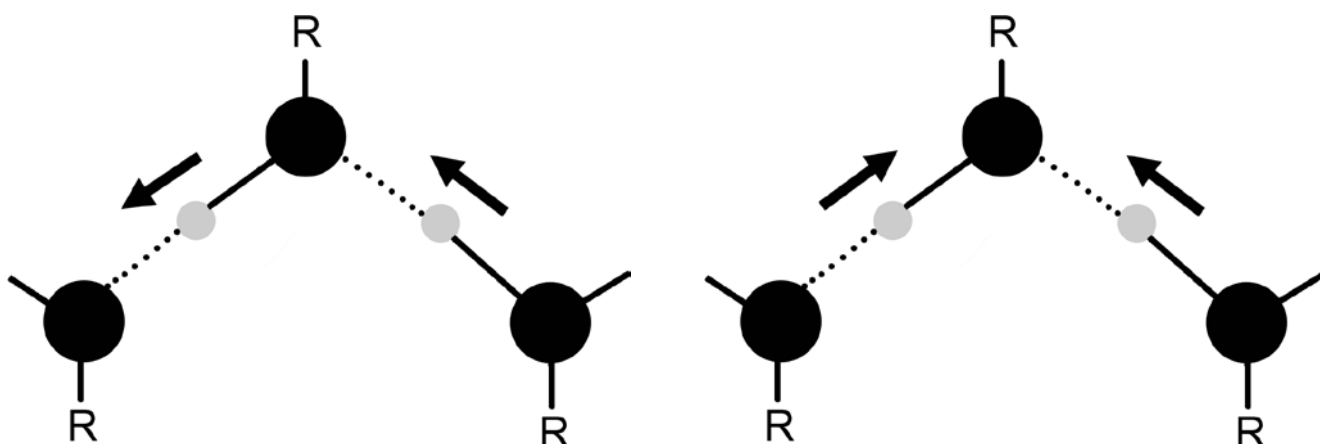
Figure S3. Schematic generalized representation of vibrations for the in-phase (left) and out-of-phase (right) coupling due to the νOH mode as occurring in a string of O-H…O hydrogen bonds; large solid and small grey balls represent oxygen and hydrogen atoms, respectively. In the case of in-phase coupling, O-H bonds of all molecules in the string elongate or shorten simultaneously (all hydrogen atoms in all O-H…O bonds in the string move synchronously in the same direction). In the case of out-of-phase coupling, the O-H bond in one molecule elongates while the O-H bond in the neighboring molecule shortens (hydrogen atoms in neighboring O-H…O bonds move asynchronously, in opposite directions). For an illustration of the longer string of H-bonded molecules see Figure S2.
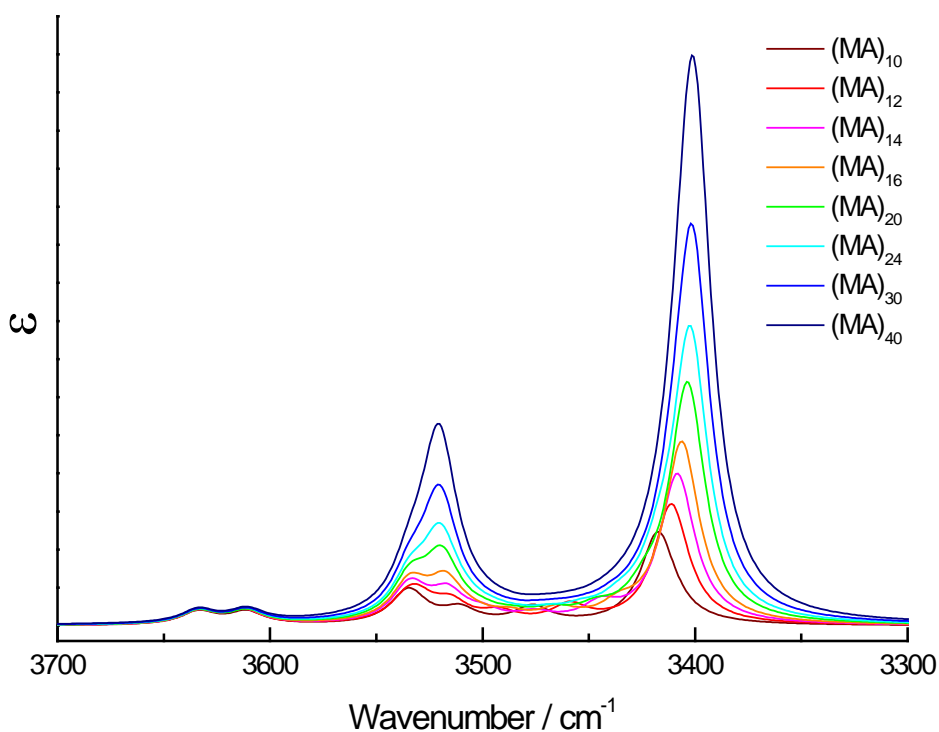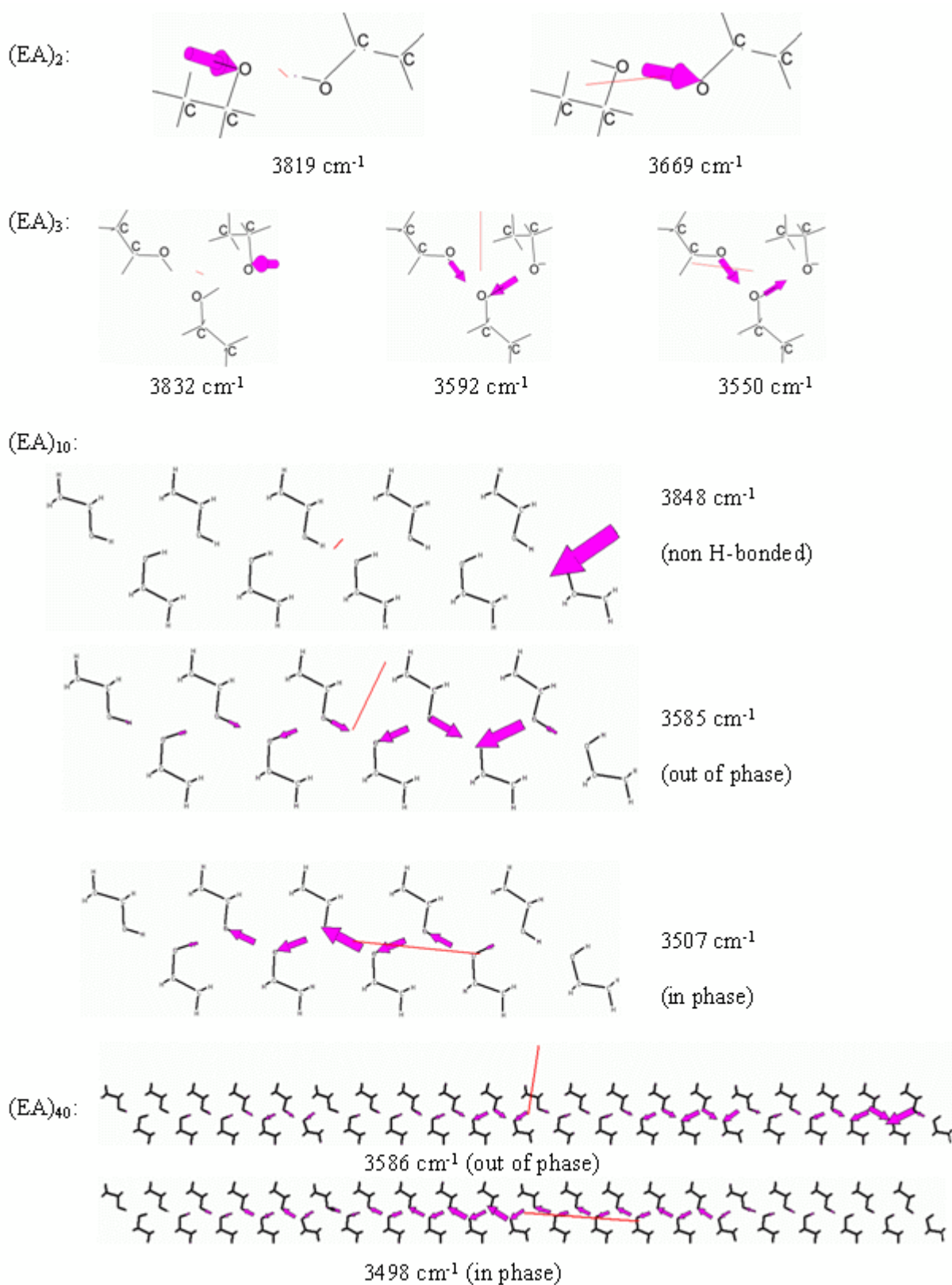

Figure S4. IR spectra in the νOH region calculated with the CCT method for different methanol models $(MA)_n$; spectral intensity is expressed as molar extinction coefficient (ε).
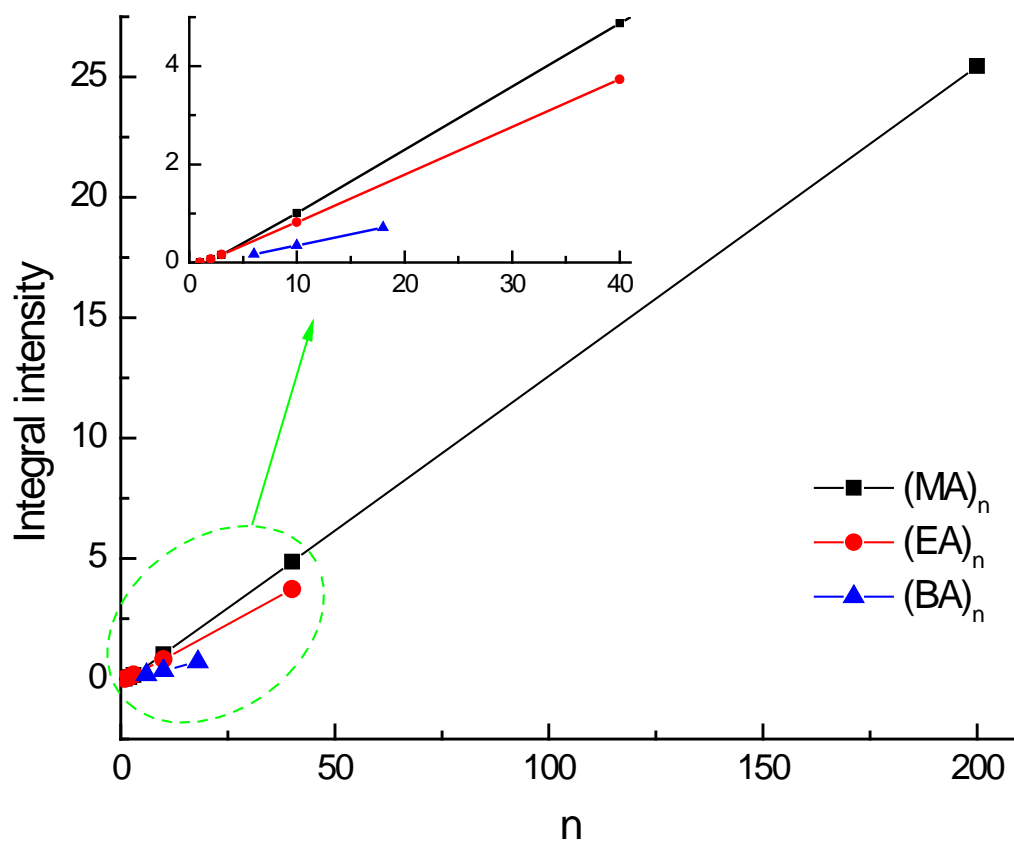
Figure S5. Calculated integral intensity of the νOH band arising from the H-bonded OH groups plotted against the number of the monomeric units (**n**) in methanol ($(MA)_n$), ethanol ($(EA)_n$) and butanol ($(BA)_n$) systems; the calculations were done at B3LYP/6-31++G** level for $(MA)_n$ and $(EA)_n$ and at semi-empirical PM3 level for $(BA)_n$. The CCT method was used for the systems with 40 and 200 monomeric units. The inset shows expanded scale for X-axis between n=0 and n=40.
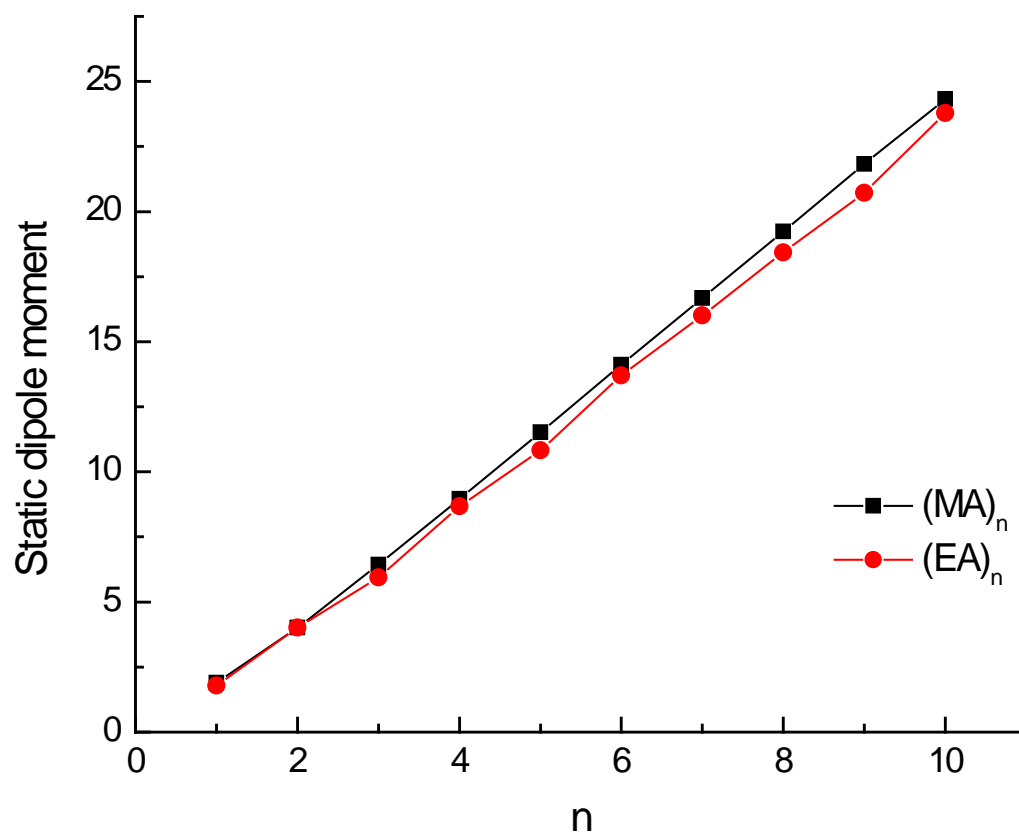
Figure S6. Magnitude of the calculated static dipole moment plotted against the number of the monomeric units (**n**) in methanol (($MA)_n$) and ethanol (($EA)_n$) models; the calculations were done at B3LYP/6-31++G** level.

(EA)₂:

3819 cm⁻¹   3669 cm⁻¹

(EA)₃:

3832 cm⁻¹   3592 cm⁻¹   3550 cm⁻¹

(EA)₁₀:

3848 cm⁻¹ (non H-bonded)

3585 cm⁻¹ (out of phase)

3507 cm⁻¹ (in phase)

(EA)₄₀:

3586 cm⁻¹ (out of phase)

3498 cm⁻¹ (in phase)

Figure S7. Displacements of selected vibrations due to the νOH normal mode (thick magenta arrows) in systems composed of two, three, ten and 40 ethanol molecules; only trans-*gauche* conformation is presented. The red lines show the directions of resulting O-H transition dipole moments.
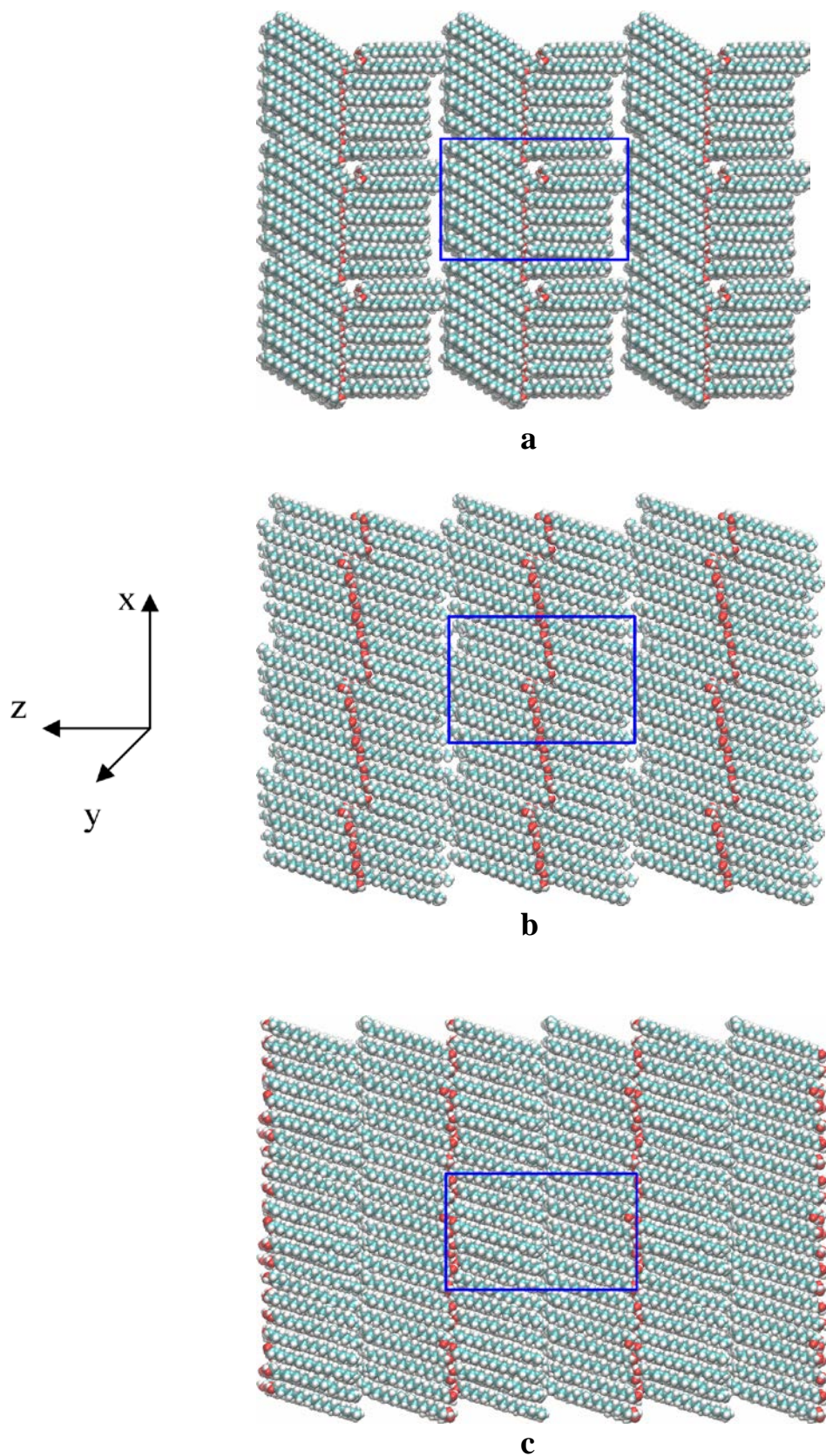
Figure S8. Van-der-Waals representation of 9 periodic boundary condition (PBC) cells after 20 ns of MD simulation for trans-trans (**a**) and trans-*gauche* (**b**) models of γ-form, and for β-form (**c**); the PBC box used in the simulations is marked in blue. The front (*xz*) view is shown for all structures.
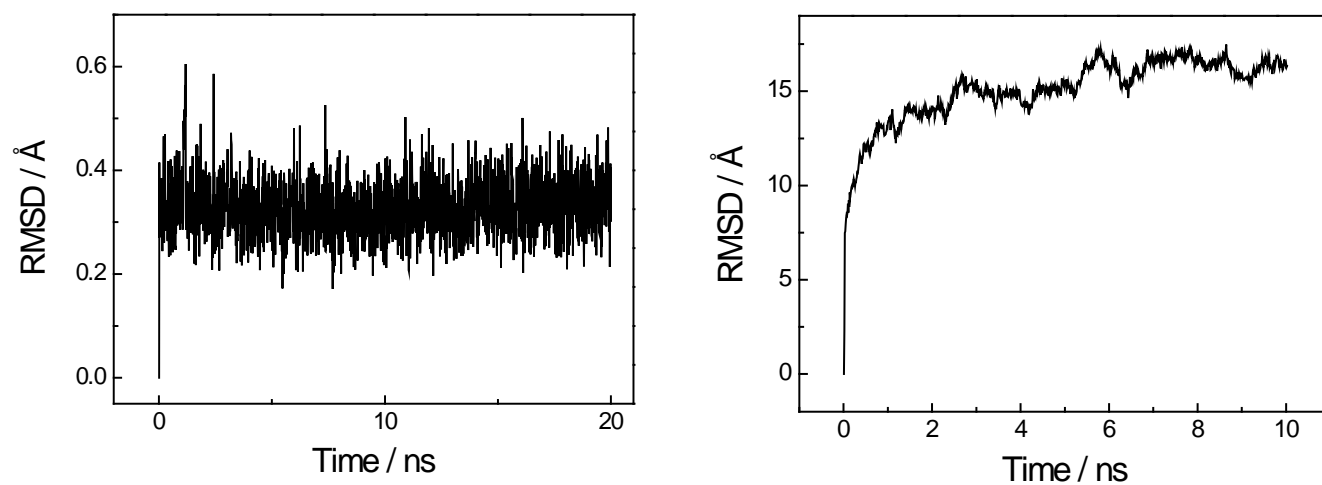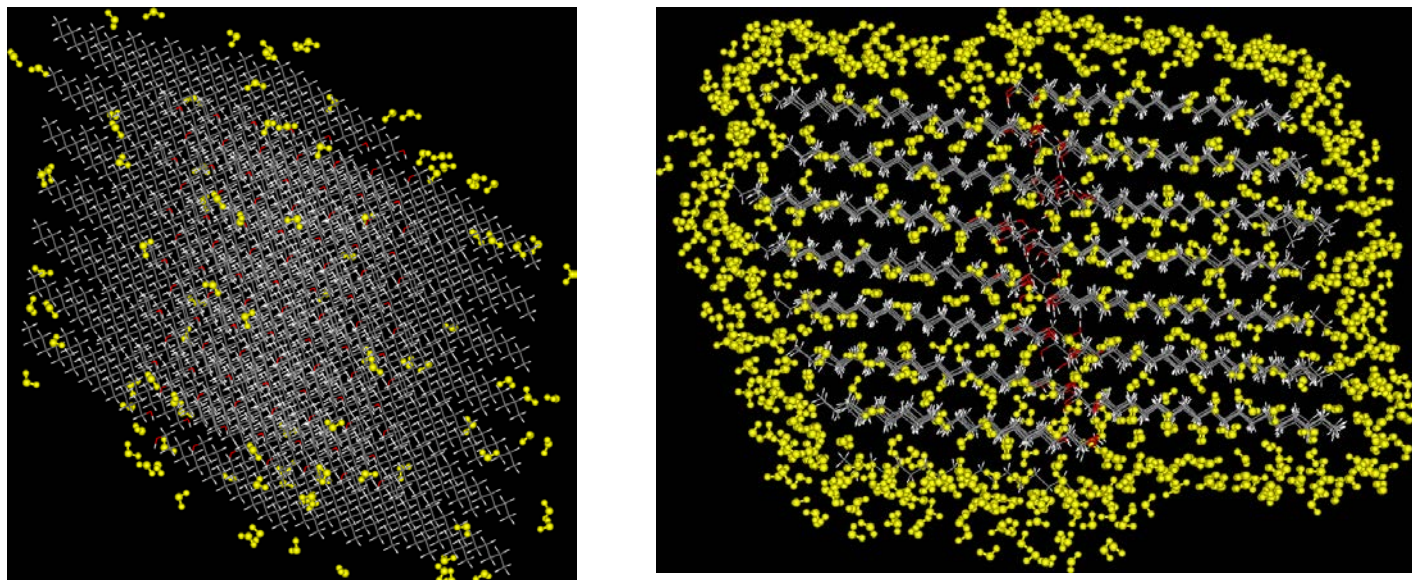
Figure S9. RMSD plots for the MD runs for (ODA)$_{98}$ trans-*gauche* model of γ-form (left) and (DOG)$_{10}$ (right).
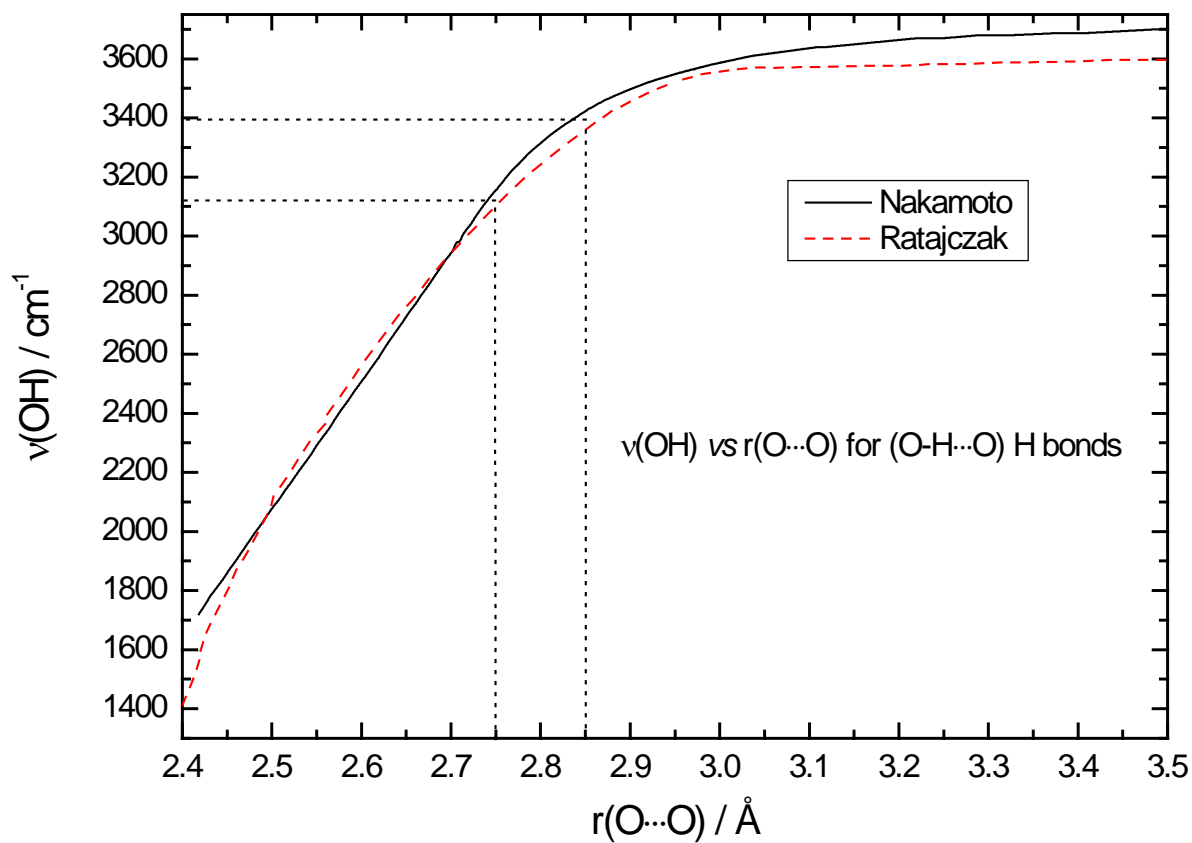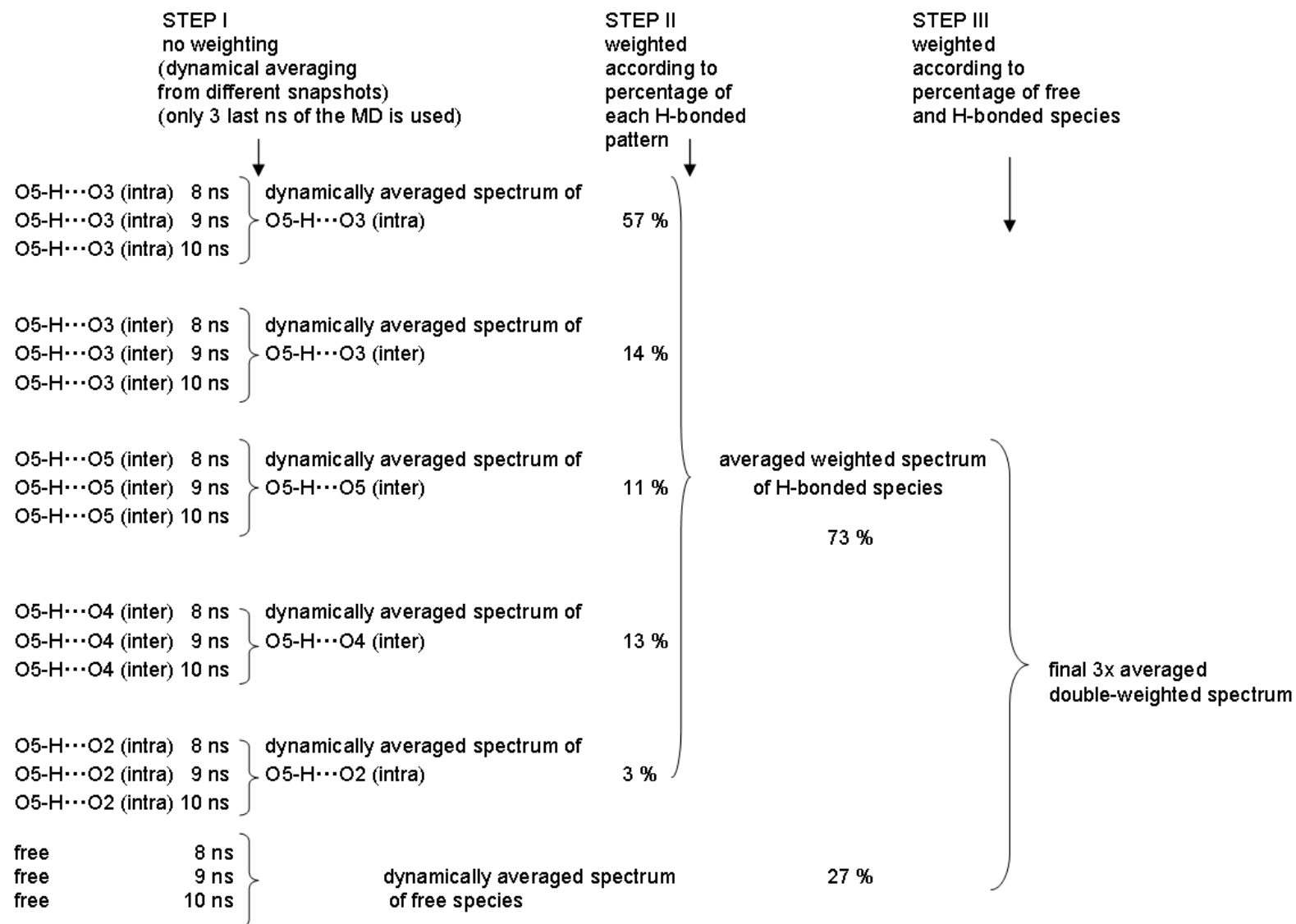
Figure S10. Summarized and digitized literature data for ν(OH) vs r(O⋯O).[33, 34] The dotted straight lines show the range of (O⋯O) distances obtained from the MD data for (ODA)$_{98}$ trans-*gauche* model of γ-form and corresponding range of ν(OH) vibration wavenumbers.

Figure S11. Starting structures for the MD simulations of the hydration of (ODA)$_{98}$ bilayer in the trans-*gauche* model of γ-form with 1 water molecule (left) and 10 water molecules per amphiphile (fully hydrated system; right).

STEP I
no weighting
(dynamical averaging
from different snapshots)
(only 3 last ns of the MD is used)

STEP II
weighted
according to
percentage of
each H-bonded
pattern

STEP III
weighted
according to
percentage of free
and H-bonded species

O5-H···O3 (intra) 8 ns
O5-H···O3 (intra) 9 ns   dynamically averaged spectrum of
O5-H···O3 (intra) 10 ns   O5-H···O3 (intra)   57 %

O5-H···O3 (inter) 8 ns
O5-H···O3 (inter) 9 ns   dynamically averaged spectrum of
O5-H···O3 (inter) 10 ns   O5-H···O3 (inter)   14 %

O5-H···O5 (inter) 8 ns
O5-H···O5 (inter) 9 ns   dynamically averaged spectrum of
O5-H···O5 (inter) 10 ns   O5-H···O5 (inter)   11 %

averaged weighted spectrum
of H-bonded species

73 %

O5-H···O4 (inter) 8 ns
O5-H···O4 (inter) 9 ns   dynamically averaged spectrum of
O5-H···O4 (inter) 10 ns   O5-H···O4 (inter)   13 %

final 3x averaged
double-weighted spectrum

O5-H···O2 (intra) 8 ns
O5-H···O2 (intra) 9 ns   dynamically averaged spectrum of
O5-H···O2 (intra) 10 ns   O5-H···O2 (intra)   3 %

free   8 ns
free   9 ns   dynamically averaged spectrum   27 %
free   10 ns   of free species

Figure S12. Schematic representation of the averaging steps to generate simulated $(DOG)_{10}$ spectra. The originally computed spectra were averaged in three steps: (i) for each of the 5 H-bond patterns and for the free molecules, the spectra obtained from different randomly chosen snapshots were averaged with equal weight for the last 3 ns of the simulation (8-10ns) to represent the dynamics of the system; (ii) the resulting spectra for all the H-bonded species were weighted according to their relevant percentage populated during the MD run, which provided a spectrum arising from all the H-bonded molecules; (iii) the resulting spectrum of the H-bonded species from the step (ii) along with the resulting spectrum of the free species from the step (i) were again weighted according to the percentage of H-bonded and free molecules. For simplicity, the H-bonded species occurring < 2% in step (ii) are not shown but used in the calculations. The final result was compared with the experimental DOG spectrum (see text).
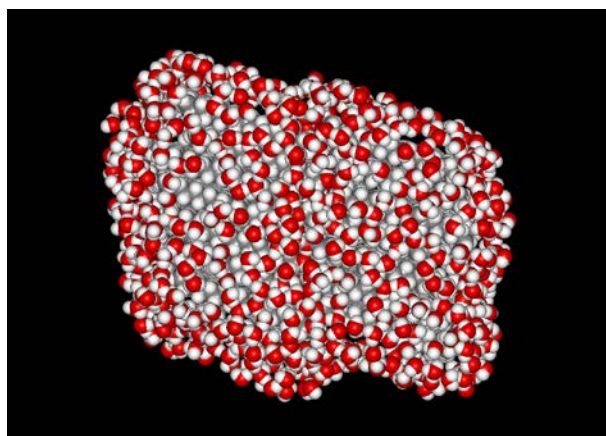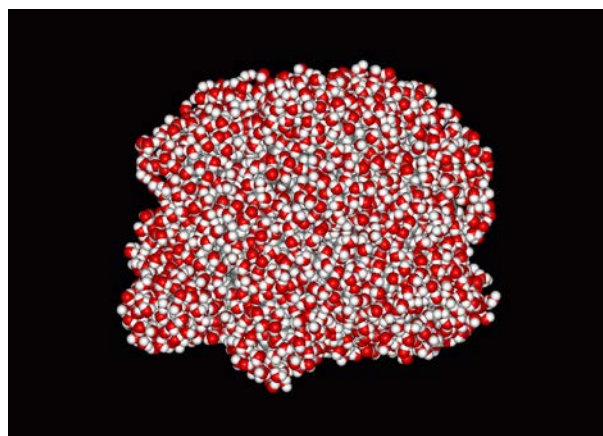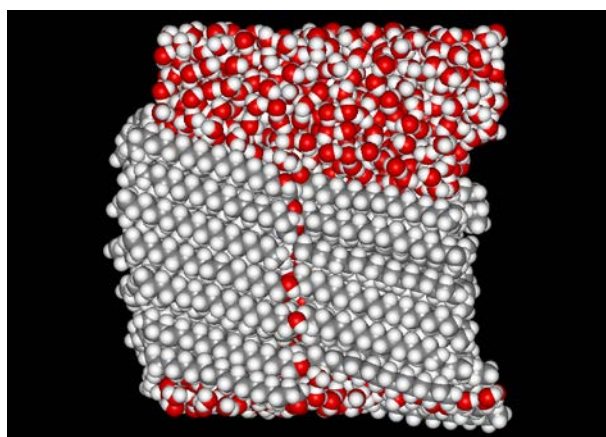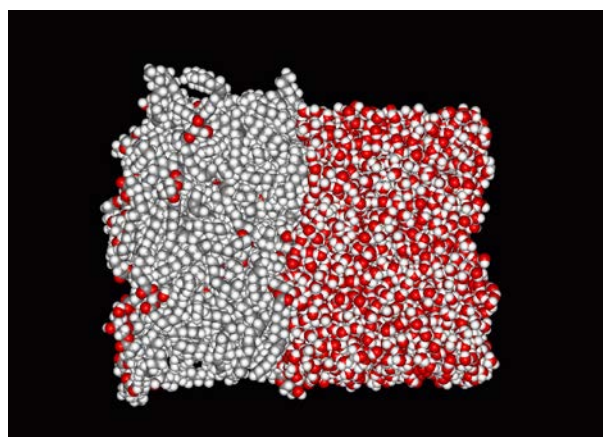
Figure S13. Comparison of the hydration of (ODA)$_{98}$ (left) and (DOG)$_{60}$ (right)[22] assemblies obtained from the MD simulations; fully hydrated systems (obtained by adding 10 water molecules per ODA and 40 water molecules per DOG amphiphile) were used. Starting geometries are shown in panels (**a**) and (**b**). The snapshots after 5 ns of MD simulations under periodic boundary conditions are shown in panels (**c**) and (**d**).

References

1.   D. S. Wishart, D. Tzur, C. Knox, R. Eisner, A. C. Guo, N. Young, D. Cheng, K. Jewell, D. Arndt, D. Sawhney, C. Fung, L. Nikolai, M. Lewis, M. Coutouly, I. Forsythe, P. Tang, S. Shrivastava, K. Jeroncic, P. Stothard, G. Amegbey, D. Block, D. D. Hau, J. Wagner, J. Miniaci, M. Clements, M. Gebremedhin, N. Guo, Y. Zhang, G. E. Duggan, G. D. MacInnis, A. M. Weljie, R. Dowlatabadi, F. Bamforth, D. Clive, R. Greiner, L. Li, T. Marrie, B. D. Sykes, H. J. Vogel and L. Querengesser, *Nucleic Acids Res.*, 2007, **35**, D521–D526.
2.   P. Bouř and P. Maloň, *MCM Molecular Graphics*, Academy of Sciences: Prague, 1995-2011.
3.   S. Abrahamsson, G. Larsson and E. Vonsydow, *Acta Crystallogr.*, 1960, **13**, 770-774.
4.   D. A. Case, T. A. Darden, T. E. Cheatham III, C. L. Simmerling, J. Wang, R. E. Duke, R. Luo, K. M. Merz, D. A. Pearlman, M. Crowley, R. C. Walker, W. Zhang, B. Wang, S. Hayik, A. Roitberg, G. Seabra, K. F. Wong, F. Paesani, X. Wu, S. Brozell, V. Tsui, H. Gohlke, L. Yang, C. Tan, J. Mongan, V. Hornak, G. Cui, P. Beroza, D. H. Mathews, C. Schafmeister, W. S. Ross and P. A. Kollman, *AMBER 9*, University of California: San Francisco, 2006.
5.   L. Rosso and I. R. Gould, *J. Comput. Chem.*, 2008, **29**, 24-37.
6.   B. Jojart and T. A. Martinek, *J. Comput. Chem.*, 2007, **28**, 2051-2058.
7.   S. W. I. Siu, R. Vacha, P. Jungwirth and R. A. Bockmann, *J. Chem. Phys.*, 2008, **128**, 125103.
8.   C. I. Bayly, P. Cieplak, W. D. Cornell and P. A. Kollman, *J. Phys. Chem.*, 1993, **97**, 10269-10280.
9.   M. J. Frisch, G. W. Trucks, H. B. Schlegel, G. E. Scuseria, M. A. Robb, J. R. Cheeseman, G. Scalmani, V. Barone, B. Mennucci, G. A. Petersson, H. Nakatsuji, M. Caricato, X. Li, H. P. Hratchian, A. F. Izmaylov, J. Bloino, G. Zheng, J. L. Sonnenberg, M. Hada, M. Ehara, K. Toyota, R. Fukuda, J. Hasegawa, M. Ishida, T. Nakajima, Y. Honda, O. Kitao, H. Nakai, T. Vreven, J. A. Montgomery Jr., J. E. Peralta, F. Ogliaro, M. Bearpark, J. J. Heyd, E. Brothers, K. N. Kudin, V. N. Staroverov, R. Kobayashi, J. Normand, K. Raghavachari, A. Rendell, J. C. Burant, S. S. Iyengar, J. Tomasi, M. Cossi, N. Rega, J. M. Millam, M. Klene, J. E. Knox, J. B. Cross, V. Bakken, C. Adamo, J. Jaramillo, R. Gomperts, R. E. Stratmann, O. Yazyev, A. J. Austin, R. Cammi, C. Pomelli, J. W. Ochterski, R. L. Martin, K. Morokuma, V. G. Zakrzewski, G. A. Voth, P. Salvador, J. J. Dannenberg, S. Dapprich, A. D. Daniels, O. Farkas, J. B. Foresman, J. V. Ortiz, J. Cioslowski and D. J. Fox, *Gaussian 09*, Gaussian, Inc.: Wallingford CT, 2009.
10.   W. L. Jorgensen, J. Chandrasekhar, J. D. Madura, R. W. Impey and M. L. Klein, *J. Chem. Phys.*, 1983, **79**, 926-935.
11.   A. D. Becke, *J. Chem. Phys.*, 1993, **98**, 1372-1377.
12.   P. Daněček and P. Bouř, *J. Chem. Phys.*, 2007, **126**, 224513.
13.   M. L. Senent, Y. G. Smeyers, R. Dominguez-Gomez and M. Villa, *J. Chem. Phys.*, 2000, **112**, 5809-5819.
14.   P. J. Stephens, *J. Phys. Chem.*, 1985, **89**, 748-752.
15.   J. R. Cheeseman, M. J. Frisch, F. J. Devlin and P. J. Stephens, *Chem. Phys. Lett.*, 1996, **252**, 211-220.
16.   P. J. Stephens, *J. Phys. Chem.*, 1987, **91**, 1712-1715.
17.   P. Bouř, J. Sopková, L. Bednárová, P. Maloň and T. A. Keiderling, *J. Comput. Chem.*, 1997, **18**, 646-659.
18.   V. Andrushchenko and P. Bouř, *Chirality*, 2010, **22**, E96-E114.
19.   V. Andrushchenko, D. Tsankov, M. Krasteva, H. Wieser and P. Bour, *J. Am. Chem. Soc.*, 2011, **133**, 15055-15064.
20.   V. Andrushchenko, L. Benda, O. Pav, M. Dracinsky and P. Bour, *J. Phys. Chem. B*, 2015, **119**, 10682-10692.
21.   J. M. Martinez and L. Martinez, *J. Comput. Chem.*, 2003, **24**, 819-825.
22.   D. R. Gauger, V. V. Andrushchenko, P. Bour and W. Pohle, *Anal. Bioanal. Chem.*, 2010, **398**, 1109-1123.
23.   A. Onufriev, D. Bashford and D. A. Case, *Proteins-Structure Function and Bioinformatics*, 2004, **55**, 383-394.
24.   G. Sigalov, P. Scheffel and A. Onufriev, *J. Chem. Phys.*, 2005, **122**, 094511.
25.   V. Andrushchenko, *Ptraj HBOND*, Prague, 2009.

26. P. Lalanne, J. M. Andanson, J. C. Soetens, T. Tassaing, Y. Danten and M. Besnard, *J. Phys. Chem. A*, 2004, **108**, 3902-3909.
27. M. G. Batishcheva, *Inzhen.-Fiz. Zh.*, 1959, **2**, 101-104.
28. M. Tasumi, T. Shimanouchi, A. Watanabe and R. Goto, *Spectrochimica Acta*, 1964, **20**, 629-666.
29. H. H. Eysel and J. E. Bertie, *J. Mol. Struct.*, 1986, **142**, 227-230.
30. W. Pohle, C. Selle, W. Rettig, U. Heiser, B. Dobner and S. Wartewig, *Arch. Biochem. Biophys.*, 2001, **396**, 151-161.
31. C. J. Pouchert, *The Aldrich Library of FT-IR Spectra*, Aldrich Chem. Co., Inc., Milwaukee, 1 edn., 1985.
32. *Journal*.
33. K. Nakamoto, M. Margoshes and R. E. Rundle, *J. Am. Chem. Soc.*, 1955, **77**, 6480-6486.
34. H. Ratajczak and W. J. Orville-Thomas, *J. Mol. Struct.*, 1968, **1**, 449-461.